RSC Advances

PAPER

View Article Online
View Journal | View Issue

Cite this: *RSC Adv.*, 2023, **13**, 11037

Discovery of nontriterpenoids from the rot roots of *Panax notoginseng* with cytotoxicity and their molecular docking study and experimental validation†

Jia-Huan Shang,[ab] Yi-Jun Qiao,[a] Hong-Tao Zhu,[a] Dong Wang,[a] Chong-Ren Yang[a] and Ying-Jun Zhang *[a]

Panax notoginseng (*PN*) is a well-known traditional Chinese medicine, with dammarane-type triterpenoid saponins characterized as major component and active ingredients, together with amino acids, flavonoids, polysaccharides, and polyacetylenes. The roots of *PN* are susceptible to root rot disease, which causes a huge loss and changes in the chemical components of this precious resource. In this study, sub-fractions of rot *PN* root extracts were preliminarily found to have admirable cytotoxicity on two human cancer cells. Further bioassay-guided isolation discovered nine new non-triterpenoids, including two novel *N*-methylacetamido-1-oxotetrahydropyrimidine alkaloids (**1**, **2**), five 2*H*-furanones or 2*H*-pyranones (**3**–**7**), and two polyacetylenic alcohols (**8**, **9**). Their structures were illuminated by extensive spectroscopic data, calculated ECD, and X-ray diffraction analysis. Among them, **3**–**7** were considered to be transformed from panaxatriol through the intermediates (**8**, **9**). The new alkaloids (**1**, **2**) displayed noteworthy cytotoxicity against five human cancer cells with IC_{50} values ranging from 14 to 24 μM. *In silico* target prediction and molecular docking studies showed that **1** and **2** may interact with EGFR, and were verified by the experimental inhibitory effect on EGFR tyrosine kinase.

Received 2nd February 2023
Accepted 17th March 2023

DOI: 10.1039/d3ra00720k

rsc.li/rsc-advances

Introduction

Panax notoginseng (Burk.) F. H. Chen (*PN*) is a famous medicinal herb belonging to the ginseng family (Araliaceae). The roots, possessing dammarane-type triterpenoid (DTT) as dominant chemical components with various bioactivities, such as immunostimulatory, anti-atherosclerotic, anti-hypertensive, antitumor, and CNS-protective activities, are used widely as major ingredients in many traditional Chinese medicinal preparation for treating cardiovascular diseases in the world.[1] Moreover, some minor constituents are also identified from *PN*. For example, dencichine, a *PN* amino acid, plays a main hemostatic role by improving the amount and activation of platelet and inhibiting fibrinolysis.[2] Polyacetylenes, found in *PN* and Korean ginseng, displayed cytotoxic, anti-platelet, and anti-microbial activities.[3]

The root rot disease has become the most severe destructive problem for *PN* cultivation, causing a huge loss and great changes in the chemical components.[4] In order to exploit *PN* resources further and discover a new bioactive skeleton, several highly oxidized dammarane-type triterpenes with favorable anticancer and anti-inflammatory activities were obtained from the rot *PN* root extracts previously by our group.[5] Continuing study showed that the remaining fractions displayed significant cytotoxicity against lung cancer A-549 and hepatocellular carcinoma cancer SMMC7721 cells (inhibition rates > 96%) at a concentration of 100 μg mL^{-1} *via* MTS assay. Further bioassay-guided isolation yielded nine new nontriterpenoids, including two novel alkaloids (**1**, **2**), five α,β-unsaturated furanones or pyranones (**3**–**7**), and two polyacetylenic alcohols (**8**, **9**) (Fig. 1).

The alkaloids (**1**, **2**) contained a unique *N*-methylacetamido substituent on their unreported 1-oxotetrahydropyrimidine skeleton, representing the first rare non-amino acid alkaloid from ginseng plants. New lactones (**3**–**7**) were biogenetically considered to be transformed from panaxatriol (PXT), a polyacetylene naturally occurring in the genus *Panax*, through their intermediate products (**8**, **9**) by a series of reactions. Herein, the structural elucidation of nine new nontriterpenoids (**1**–**9**), the plausible bio-transformed pathway for lactones, as well as their antiproliferative activity against five human cancer cell lines, were deduced in detail. Moreover, *in silico* target prediction and

[a]*State Key Laboratory of Phytochemistry and Plant Resources in West China, Kunming Institute of Botany, Chinese Academy of Sciences, Kunming 650201, PR China. E-mail: zhangyj@mail.kib.ac.cn; Tel: +86-871-6522-3235*

[b]*University of Chinese Academy of Sciences, Beijing 100049, PR China*

† Electronic supplementary information (ESI) available: Materials, experimental details, characterization of compounds, *in vitro* and *in silico* biological study, and NMR copies of new compounds. CCDC 2096666. For ESI and crystallographic data in CIF or other electronic format see DOI: https://doi.org/10.1039/d3ra00720k

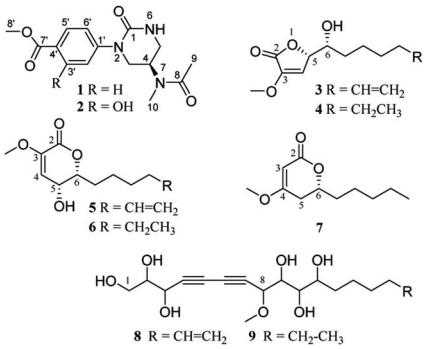

Fig. 1 Chemical structures of compounds **1–9**.

molecular docking studies were adopted to analyze the interaction of cytotoxic molecules with the predicted target protein (EGFR), which was further verified by the experimental protein inhibition assay.

Results and discussion

The methanol extract (4.0 kg) of *PN* rot root was fractionated into three main fractions (Fr. A–C), and Fr. C (220.8 g) was further divided into six sub-fractions (Fr. C1–C6) by an RP-18 CC. In our previous work, eight anti-inflammatory and anticancer triterpenes were reported from the sub-Fr. C2, C3, and C5.[5b] Further study showed that the remaining sub-Fr. C1 and C6 displayed significant cytotoxicities against lung cancer A-549 and hepatocellular carcinoma SMMC7721 cancer cells with inhibition rates exceeding 96%, while sub-Fr. C4 displayed no obvious inhibitory effect (Table S4†). Therefore, the present study mainly focused on the remaining bioactive fractions, resulting in the discovery of compounds **1**, **2**, **8**, and **9** from Fr. C1, and **3–7** from Fr. C6, respectively.

Structure elucidation of compounds 1–9

Compound **1** was obtained as a colorless needle crystal, and its molecular formula was determined to be $C_{15}H_{19}N_3O_4$ by the HRESIMS (*m*/*z* 328.1269 $[M + Na]^+$, calcd for, 328.1273), corresponding to eight degrees of unsaturation. The ^1H, ^{13}C NMR and HSQC spectra suggested the presence of *para*-substituted benzene [δ_C 147.0, 126.8, 130.5 (2C), 124.2 (2C), δ_H 7.98 and 7.33 (each 2H, d, J = 8.7 Hz)], and the remaining nine carbon resonances assignable to three conjugated ketones (δ_C 171.6, 166.8, 155.0), one methine (δ_C 46.1), two methylenes (δ_C 50.0, 42.6), two singlet methyls (δ_C 32.6, 22.6) and one methoxyl (δ_C 52.3), as well as broad and short active hydrogen (δ_H 5.63) (Table 1). The ^1H–^1H COSY correlations (Fig. 2A) of NH (δ_H 5.63)/H_2-5 (δ_H 3.53, 3.48)/H-4 (δ_H 5.04)/H_2-3 (δ_H 3.08) suggested the presence of –NH–CH_2–CH–CH_2– fragment. The HMBC (Fig. 2A) correlations from H_3-9 (δ_H 2.10), H_3-10 (δ_H 3.03), and H-4 to C-8 (δ_C 171.6), H_3-9 to C-10 (δ_C 32.6), H_3-10 to C-4 (δ_C 46.1), revealed an *N*-methyl acetylamino group located at C-4. Likewise, the HMBC correlations of H-3′/5′ (δ_H 7.98), H-2′/6′ (δ_H 7.33), and H_3-8′ (δ_H 3.87) to C-7′ (δ_C 166.8), and H_3-8′ to C-4′ (δ_C 126.8) indicated the existence of a methoxyl acyl group at C-4′. In addition, the very high field of the carbonyl group (δ_C 155.0) showed a correlation with H_2-3/H_2-5 in the HMBC spectrum, and the HMBC correlation between H_2-3 and C-1′, suggested an (*N*-methyl acetylamino)-oxytetra-hydropyrimidine ring was attached to C-1′ (δ_C 147.0) of *para*-substituted benzene through a tertiary nitrogen atom. Finally, the structure and absolute configuration of **1** were unequivocally confirmed as (*R*)-2-(*p*-benzoate methyl)-4-(*N*-methylacetami-do)-1-oxotetrahydropyrimidin by X-ray single crystal diffraction [Flack parameter = 0.03 (4)] (Fig. 2B).

Table 1 ^1H and ^{13}C NMR data for compounds **1** and **2** in $CDCl_3$[a]

	1		**2**	
No.	δ_C	δ_H	δ_C	δ_H
1	155.0		155.5	
3	50.0	3.80 dd (11.8, 7.1)	50.8	3.72 m
4	46.1	5.04 m	46.1	5.05 m
5	42.6	3.53 ddd (11.8, 5.6, 2.3) 3.48 ddd (11.8, 7.1, 1.3)	42.9	3.53 ddd (11.8, 5.6, 2.7) 3.49 ddd (11.8, 7.3, 1.5)
6		5.63 s		5.10 s
8	171.6		171.6	
9	22.6	2.10 s	22.7	2.12 s
10	32.6	3.03 s	32.6	3.06 s
1′	147.0		134.4	
2′	124.2	7.33 d (8.7)	127.0	7.70 d (2.7)
3′	130.5	7.98 d (8.7)	160.0	
4′	126.8		112.5	
5′	130.5	7.98 d (8.7)	118.5	6.95 d (8.9)
6′	124.2	7.33 d (8.7)	134.1	7.37 dd (8.9, 2.7)
7′	166.8		170.2	
8′	52.3	3.87 s	52.6	3.91 s
OH				10.67 s

[a] d: doublet; m: multiplet; s: singlet; δ in ppm; J in Hz.

Compound **2** was isolated as white amorphous powder, with a molecular formula of $C_{15}H_{19}N_3O_5$, as deduced by HREIMS (*m*/*z* 321.1328 $[M]^+$), which was one more oxygen atom than that of **1**. Their ^1H and ^{13}C NMR data showed some similarities, except for an additional broad active hydrogen (δ_H 10.67) and 1,2,4-

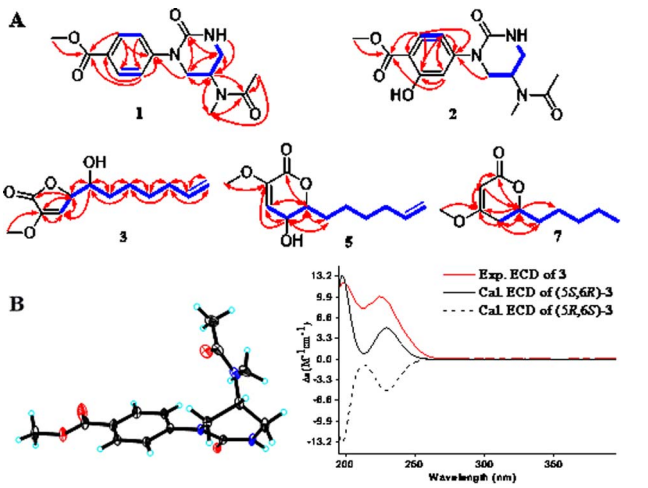

Fig. 2 (A) Key ^1H–^1H COSY (–) and HMBC (→) correlations of **1–3**, **5**, **7**. (B) (left) ORTEP of **1** with thermal ellipsoids shown at 30% probability. (right) Experimental ECD and calculated ECD spectra of **3**.

substituted benzene ring signals in **2** (Table 1). The same chemical shifts of benzoate methyl (δ_C 170.2, 52.6) and (*N*-methylacetylamino)-oxytetrahydropyrimidine ring [δ_C 155.5 (C-1), 50.8 (C-3), 46.1 (C-4), 42.9 (C-5), 171,6 (C-8), 22.7 (C-9), 32.6 (C-10)] as those of **1**, as well as the HMBC correlations between H-5′ (δ_H 6.95), H-6′ (δ_H 7.37) and C-1′ (δ_C 134.4), H-5′ and C-7′ (δ_C 170.2)/C-4′ (δ_C 112.5), H_3-8′ (δ_H 3.91) and C-7′, confirmed that two parts were connected through a tertiary nitrogen atom. The additional oxygen was assigned to a hydroxyl group at C-3′ (δ_C 160.0) because of H-2′ presenting as a smaller doublet signal (δ_H 7.70, d, 2.7 Hz) with HMBC correlation to C-1′ (Fig. 2A). On account of the only chiral carbon at C-4 in **2**, the consistent positive optical ration with **1**, indicated the same 4*R*-configuration for **2** to **1**. Thus, **2** was determined as (*R*)-2-(3-hydroxy-4-methoxyl acyl)phenyl-4-(*N*-methylacetamido)-1-oxotetrahydropyrimidin.

Compound **3** was obtained as a yellow oil, possessing a molecular formula $C_{12}H_{18}O_4$, as determined by the HRESIMS (*m*/*z* 271.1186 $[M + HCOO]^-$). The ^{13}C NMR spectrum showed 12 carbon resonances, assignable to five methylenes with a vinyl (δ_C 113.9), four methines with two oxygen bearings (δ_C 83.0, 72.0), two quaternary carbons, and one methoxyl. The ^1H NMR spectrum presented a methoxy at δ_H 3.65 (3H, s), two oxymethines at δ_H 5.04 (overlap) and 4.02 (d, 3.1 Hz), two olefinic protons at δ_H 6.58 (d, 1.7 Hz) and 5.83 (ddt, 16.9, 10.2, 6.7 Hz), and two terminal olefinic protons at δ_H 5.04 and 4.99 (dd, 10.1, 0.8 Hz) (Table 2). Analysis of the ^1H–^1H COSY correlations (Fig. 2A) revealed a chain fragment of –CH–CH(O)–CH(O)–$(CH_2)_4$–CH=CH_2. In the HMBC spectrum of **3**, correlations of olefinic proton H-4 (δ_H 6.58) with C-3 (δ_C 148.7)/C-5 (δ_C 83.0), oxymethines H-5 (δ_H 5.04) with C-2 (δ_C 168.4)/C-3/C-4 (δ_C 116.0)/C-6 (δ_C 72.0) and H-6 (δ_H 4.02) with C-4/C-5/C-7 (δ_C 34.2)/C-8 (δ_C 26.2), and the methoxyl protons (δ_H 3.65) with C-3 were observed respectively. The aforementioned evidence constructed that the planar structure of **3** as 3-methoxy-substituted α,β-unsaturated-γ-lactone with a long chain at C-5. The absolute configurations of C-5 and C-6 were determined by combining HETLOC correlations together with ECD spectrum. The ECD spectrum showed a negative Cotton effect at 210 nm for a lactone moiety, indicating the *S* configuration of C-5.[6] Furthermore, the small coupling constant of $^3J_{H5-H6}$ (3.0 Hz) indicated the *gauche* conformation for H-5 and H-6, while the two small bond heteronuclear coupling constants ($^2J_{H6-C5}$ = 2.8 Hz, $^2J_{H5-C6}$ = 2.3 Hz) in the HETLOC spectrum (Fig. S29†), suggested the relative configurations of H-5 and H-6 were *threo* and determined 5*S*,6*R* configurations of **3**.[7] Subsequent ECD calculations were conducted to further identify the absolute configuration of **3**, which showed that the calculated ECD spectrum of (5*S*,6*R*)-**3** was in good agreement with the experimental ECD curve of **3** (Fig. 2B). Consequently, compound **3** was determined as (5*S*,6*R*)-5-(1-hydroxy-2-pentenyl)-3-methoxy-2(5*H*)-furanone.

Compound **4** was isolated as a colorless oil and was assigned the molecular formula $C_{12}H_{20}O_4$ with three degrees of unsaturation by the HRESIMS (*m*/*z* 273.1345 $[M + Na]^+$). Detailed comparison of NMR data between **4** and **3** indicated their structures to be quite similar, except that the terminal ethyl group (δ_C 139.7, 115.2) in **3** was replaced by one methylene (δ_C 23.4) and one methyl group (δ_C 14.8) in **4**, as indicated by the HMBC correlations from H_2-11 (δ_H 1.25) to C-10 (δ_C 32.6)/C-12 (δ_C 14.8) and the ^1H–^1H COSY correlations of H_3-12 (δ_H 0.85)/H_2-11/H_2-10 (δ_H 1.77, 1.50)/H-9 (δ_H 1.33). Meanwhile, the HETLOC spectrum (Fig. S40†) showed small heteronuclear coupling constants ($^2J_{H6-C5}$ = 2.8 Hz, $^2J_{H5-C6}$ = 2.9 Hz), and the ECD spectrum (Fig. S43†) almost overlapped with that of **3** (Fig. S32†), indicating the 5*S*,6*R* configurations of **4**. Hence, compound **4** was concluded as (5*S*,6*R*)-5-(1-hydroxyheptyl)-3-methoxy-2(5*H*)-furanone.

Table 2 ^1H and ^{13}C data for compounds **3**–**6** in CD_3CN and **7** in CD_3OD[a]

	3		**4**		**5**		**6**		**7**	
No.	δ_C	δ_H	δ_C	δ_H	δ_C	δ_H	δ_C	δ_H	δ_C	δ_H
2	168.4		168.5		161.0		161.1		167.6	
3	148.7		148.8		145.2		145.2		90.3	5.05, s
4	116.0	6.58, d (1.7)	116.1	6.59, d (2.1)	114.9	6.00, d (3.3)	114.9	6.00, d (3.2)	173.0	
5	83.0	5.04, overlap	83.1	5.06, dd (4.8, 2.1)	66.5	4.63, m	66.6	4.65, m	33.0	2.39, ddd (17.0, 12.0, 1.1) 2.24, dd (17.0, 3.8)
6	72.0	4.02, d (3.1)	72.1	4.03, m	84.7	4.53, td (8.3, 3.2)	84.8	4.55, td (8.3, 3.3)	76.0	4.29, m
7	34.2	1.68, m	34.4	1.71, overlap	32.7	2.00, overlap 1.77, dtd (14.0, 9.5, 4.8)	32.9	2.00, m 1.78, m	34.7	1.70, m 1.55, m
8	26.2	1.77, m; 1.50, m	30.1	1.22, overlap	25.5	1.60, m; 1.43, m	25.9	1.58, m; 1.42, m	24.5	1.43, m; 1.33, m
9	29.6	1.39, m	26.7	1.33, m	29.4	1.32, m	29.8	1.24, overlap	31.6	1.19, overlap
10	34.4	2.03, m	32.6	1.77, overlap; 1.50 m	34.3	1.96, dd (14.2, 7.0)	32.3	1.14, overlap	22.5	1.24, overlap
11	139.7	5.83, ddt (16.9, 10.2, 6.7)	23.4	1.25, overlap	139.5	5.78, ddt (17.0, 10.2, 6.7)	23.2	1.19, overlap	14.0	0.81, t (7.0)
12	115.2	5.04, overlap 4.99, dd (10.2, 0.8)	14.8	0.85, t (7.0)	115.3	5.03, dd (17.0, 1.6) 4.97, m	14.7	0.81, t (7.1)	56.1	3.66, s
OMe	58.4	3.65, s	58.4	3.68, s	55.9	3.57, s	55.8	3.57, s		

[a] d: doublet; m: multiplet; s: singlet; t: triplet; δ in ppm; *J* in Hz.

Compound **5** yielded a white amorphous powder, and had the same molecular formula $C_{12}H_{18}O_4$ as that of **3**, evidenced by the HRESIMS data at *m*/*z* 271.1186 $[M + HCOO]^-$. The detailed analysis of ^1H and ^{13}C NMR, DEPT, and HSQC spectra showed varied different chemical shifts with those of **3** on the two oxymethines as well as the *α*,*β*-unsaturated ketone carbons. The HMBC correlations from oxymethines H-6 (δ_H 4.53) to C-2 (δ_C 161.0)/C-4 (δ_C 114.9)/C-5 (δ_C 66.5)/C-7 (δ_C 32.7)/C-8 (δ_C 25.5) and H-5 (δ_H 4.63) to C-3 (δ_C 145.2)/C-4/C-6 (δ_C 84.7), as well as the ^1H–^1H COSY correlations of H-4/H-5/H-6/H_2-7 (δ_H 2.00, 1.77)/H_2-8 (δ_H 1.60, 1.43)/H_2-9 (δ_H 1.32)/H_2-10 (δ_H 1.96)/H-11 (δ_H 5.78)/H_2-12 (δ_H 5.03, 4.97), revealed a six-membered *δ*-lactone in **5** replacing the *γ*-lactone moiety in **3**. According to the small coupling constant of $^3J_{H5-H6}$ (3.2 Hz), and a reliable ECD empirical rule for structure with *α*,*β*-unsaturated-*δ*-lactone moiety,[8] 6*R* Configuration was assigned as the ECD spectrum of **5** (Fig. S53†) showing a positive Cotton effect at 262 nm. Thus, compound **5** was elucidated as (5*R*,6*R*)-6-(1-hydroxy-5-hexenyl)-5-hydroxy-3-methoxy-2(5*H*)-pyranone.

Compound **6** was obtained as a yellow amorphous powder with the same molecular formula $C_{12}H_{20}O_4$ as that of **4**, suggested by a molecular ion peak at *m*/*z* 273.1345 $[M + HCOO]^-$. The NMR data (Table 2) characterized an identical *α*,*β*-unsaturated-*δ*-lactone moiety (δ_C 161.1, 145.2, 114.9, 84.8, 66.6) with **5**. The slight difference between them was that the terminal alkenyl (δ_C 139.5, 115.3) chain in **5** was reduced to an aliphatic chain at C-6, as the ^1H–^1H COSY spectrum showing the long coherent signals of H-3/H-4/H-5/H_2-6/H_2-7/H_2-8/H_2-9/H_2-10/H_3-11 in **6**. Moreover, the consistency between the ECD spectra of compounds **6** and **5** and the small $J_{H4/H5}$ (3.3 Hz), indicated that **6** shared the same 5*R* and 6*R* configurations with that **5**. Thus, the structure of **6** was determined to be (5*R*,6*R*)-6-(1-hydroxyhextyl)-5-hydroxy-3-methoxy-2(5*H*)-pyranone.

Compound **7** was isolated as a colorless oil and its molecular formula $C_{11}H_{18}O_3$ was deduced from HRESIMS (*m*/*z* 221.1149 $[M + Na]^+$). The ^{13}C NMR and DEPT spectra showed 11 carbons, which were similar to those of **6**, except for a set of up and down-shifted double bond signals (δ_C 90.3, 173.0 for **7**; δ_C 145.2, 114.9 for **6**) and a missing oxymethine in **7**. The ^1H–^1H COSY correlations of H_2-5/H-6/H_2-7/H_2-8/H_2-9/H_2-10/H_3-11 and HMBC correlations of H-6 with C-2/C-4/C-5/C-7/C-8, H_2-5 with C-3/C-4/C-6/C-7, H-3 with C-2/C-4/C-6, and methoxyl protons (δ_H 3.66) with C-4, established the plane structure of **7**. Moreover, the optical rotation of **7** ([*a*] −97.4) was consistent with a synthesized analogue (*R*)-6-hexyl-4-methoxy-6-hydroxy-2*H*-pyran-2-one ([*a*] −103.5, >99% ee)[9] and opposite to the corresponding isomer ([*a*] +80.1, 83% ee) with the identical skeletal structure to **7** but surplus *S*-isomer,[10] indicating *R*-configuration for **7**. Therefore, compound **7** was identified (*R*)-6-(1-hydroxyhextyl)-4-methoxy-2(5*H*)-pyranone.

Compounds **8** and **9** were isolated as both colorless oil and had molecular formulas of $C_{18}H_{28}O_7$ and $C_{18}H_{30}O_7$, respectively. Their 1D NMR and HSQC spectra showed great similarities, except that an alkenyl in **8** was replaced by an aliphatic methyl in **9** (Table S1†). The ^1H–^1H COSY spectrum displayed clear –CH_2(O)–CH(O)–CH(O)– (**8** and **9**)– and –$(CH_2)_4$–CH=CH_2 (**8**) or –$(CH_2)_5$–CH_3 (**9**) correlations, and the HMBC correlations of H-8 with C-7/C-6/C-5/C-4/OCH_3, H-9 with C-7, H-3 with C-4/C-5/C-6/C-7, H-2 with C-4, and methoxy proton (δ_H 3.46) with C-8, indicating the partial structure of C-1 to C-9 connected by the conjugate diacetylene and a methoxy group located at C-8 in both **8** and **9**. Six broad active protons (OH) peaks in the downfield showed direct ^1H–^1H COSY correlations with H-1 to H-3, and H-9 to H-11, respectively, evidenced further the existence and location of six hydroxyls. Thus, the planar structures of **8** and **9** were identified, as shown in Fig. 1. Regrettably, the absolute configurations of **8** and **9** were undetermined because of the polyhydroxyl substitution on their flexible skeleton.

Plausible bio-transformed pathways for 3–6, 8, and 9

Panaxytriol (PXT), widely existing in *Panax* species, was also found in the infected *PN* roots in the present study, and its absolute configuration was identified as 3*R*,9*R*,10*R* by circular dichroism (CD) analysis[11] and synthetic method.[12] Based on the structure of natural PXT and the obtained intermediates (**8**, **9**), a plausible transformation pathway from PXT to four lactones (**3**–**6**) is proposed in Scheme 1. Under the high degree of oxidization in the infected plant, the olefinic bond, C-8, C-11, and terminal fatty chain of natural PXT were selectively oxidized to intermediate products (**8**, **9**). Their second alkynyl (C-6, C-7) was then oxidatively cracked into the carboxyl group, which was further esterified with one of the hydroxyl groups randomly to form a five- or six-member lactone ring. Finally, the hydroxyl group next to methoxy was eliminated with *ortho* hydrogen to form a double bond. The absolute configuration of C-10 on PXT and lactones were kept unchanged during the transformation. In turn, the identification of 6*R*-configuration on compounds **3**–**6** proved the outstanding stereoselectivity of the oxidization reaction by bio-catalysis. To the best of our knowledge, only a few studies have reported that PXT can be transformed into new metabolites by fungi.[13] New lactones and their precursors discovered in this work suggested that polyacetylene in *PN* could also be transformed under a highly oxidized environment, and the endophyte in the rot *PN* roots could be a potential tool to convert PXT and ginsenosides, which was worth further investigation.

In vitro cytotoxic activity

All the isolates were evaluated for cytotoxicity on five human cancer cell lines (myeloid leukemia HL-60, lung cancer A-549, colon cancer SW480, breast cancer MCF-7, and hepatocellular

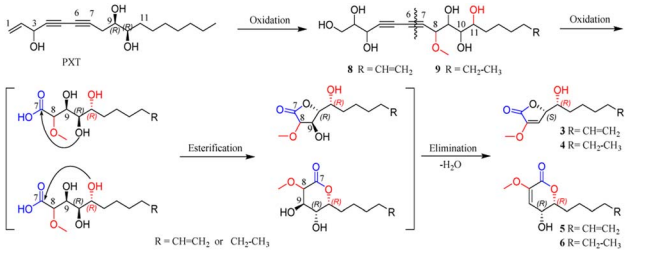

Scheme 1 Plausible bio-transformed pathway for **3**–**6**, **8**, and **9**.

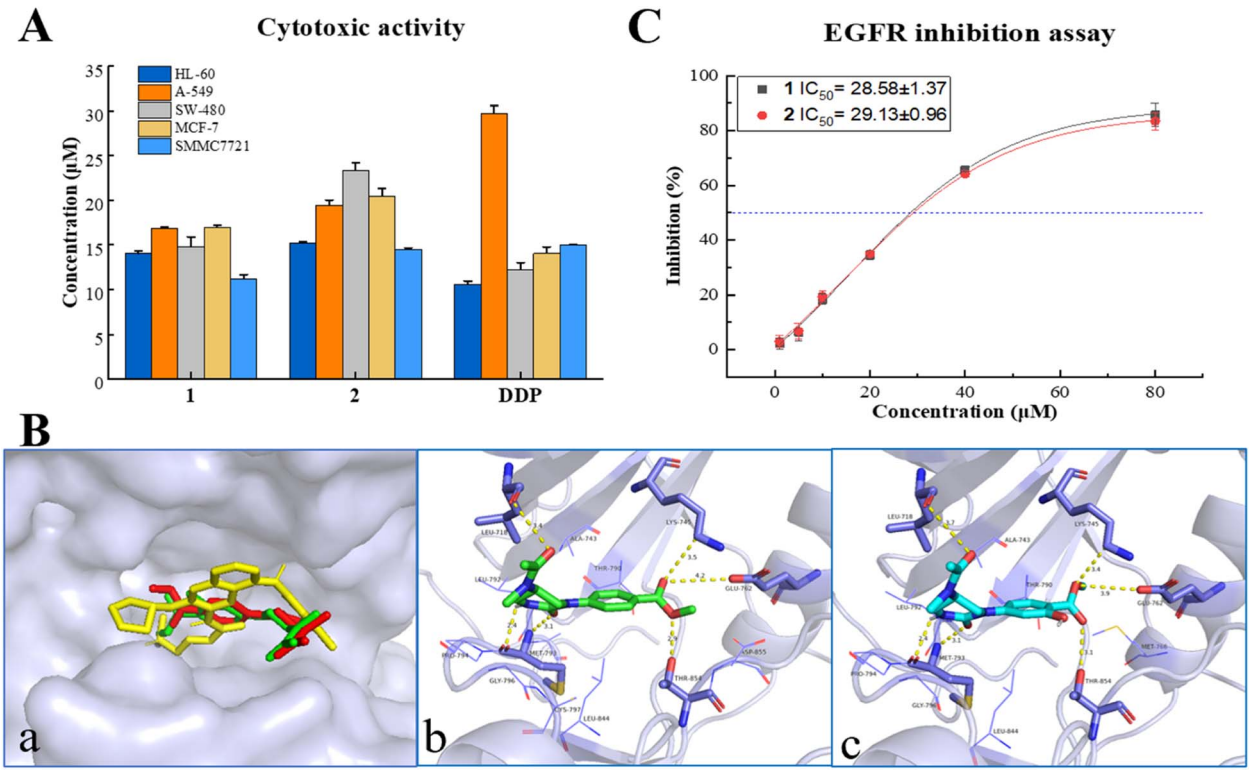

Fig. 3 (A) Cytotoxicities of **1** and **2**. (B) Molecular docking on EGFR: (a) Overlay docking positions of **1** (red), **2** (green), and afatinib (yellow) in the active site of EGFR (surface model). (b and c) The binding mode between EGFR and **1**, **2**, respectively. (C) IC_{50} values of EGFR inhibition for **1** and **2**.

carcinoma SMMC7721, purchased from ATCC (American Type Culture Collection), USA) by the MTS method. As shown in Fig. 3A and Table S5,† two alkaloids (**1**, **2**) displayed a promising inhibitory activity against all five cancer cells with IC_{50} values ranging from 14–24 μM, which were comparable with that of positive control cisplatin (DDP, purchased from Selleck, USA). However, all the α,β-unsaturated lactones (**3**–**7**) showed no significant cytotoxicity on tested cancer cells with inhibition ratios < 50% at a concentration of 40 μM (Table S4†). This is different from the previous research on their precursor structure (PXT).[3a,b] The results of the *in vitro* bioassay suggested that endophytes in the infected *PN* roots may hold a detoxification mechanism, which can convert toxic metabolites into less toxic compounds to make themself survive in the rhizosphere environment.

In silico target prediction and molecular docking analysis

In silico studies nowadays play an important role in small molecule target prediction and help novel structures to find bioactive potential.[14] To explore the possible target protein and obtain deeper insights into the intermolecular recognition mode, target prediction, and molecular docking simulation were performed.

Of all the top 15 possible targets predicted by SwissADME for **1** and **2**, epidermal growth factor receptor (EGFR), directly or indirectly related to the world's most common and deadly cancers, was investigated for molecular docking study. EGFR belongs to a family of four related receptor tyrosine kinases, which act as key mediators in cell signaling pathways involving cell proliferation, apoptosis, angiogenesis, and metastatic spread.[15] As depicted in Fig. 3B, **1**, **2**, and the EGFR inhibitor, afatinib, were docked exactly on the ATP binding pocket of wild human EGFR tyrosine kinase (PDB: 6VHN). The EGFR/**1** complex revealed a good least binding energy of −6.6 kcal mol^{-1}, higher than that of the positive control, afatinib (−7.3 kcal mol^{-1}). The binding profile of **1** showed that C-1, C-8 carbonyl groups interacted with MET 793 (3.1 Å) and LEU 718 (3.4 Å), 6-NH interacted with MET 793 (2.4 Å), 8′-O atom interacted with THR 854 (2.9 Å), C-7′ carbonyl group interacted with LYS 745 (3.5 Å), and GLU 762 (4.2 Å) (the same residues binding with co-crystallized ligand). Compound **2** displayed almost the same binding mode of **1** on the receptor site with a binding energy of −6.5 kcal mol^{-1} through several hydrogen bonds between C_1═O and MET 793 (3.1 Å), C_8═O and LEU 718 (3.7 Å), 6-NH and Met 793 (2.4 Å), 8′-O and THR 854 (3.1 Å), $C_{7'}$ = O and LYS 745 (3.4 Å), GLU 762 (3.9 Å). The adopted molecular docking method was verified by redocking the co-crystallized ligand with small RMSD = 0.68 Å and a binding energy score of −7.6 kcal mol^{-1}. In addition, physicochemical parameters for both Lipinski's and Veber's rules and pharmacokinetic properties (gastrointestinal absorption and blood–brain barrier) were determined for **1**, **2**, and afatinib proceeding by SwissADME.[16] As shown in Table S7,† **1** and **2** obeyed the rule of five (RO5) criteria without any violations from Lipinski's Rule and passed through the Veber rule by topological polar surface area (TPSA) lower than 140 Å^2. Meanwhile, compounds **1**, **2**, and afatinib

showed high gastrointestinal absorption with no permeation to the blood–brain barrier. The new compounds **1** and **2** exhibited not only anti-proliferative activity but also promising oral bioavailability pharmacokinetic properties as the positive control, afatinib.

EGFR tyrosine kinase inhibition activity

EGFR overexpression is observed in cancers of the head and neck, ovary, cervix, bladder, oesophagus, stomach, brain, breast, endometrium, colon, and lung.[17] The activation and autophosphorylation of intracellular tyrosine kinase domain of the receptors lead to several downstream signaling pathways, therewith eliciting the cascade of multiple events in the cytoplasm, as well as cell proliferation, survival, and apoptosis.[18] International guidelines recommended EGFR inhibitors as the priority treatment for advanced EGFR mutation patients, regarding the higher efficacy and safety rather than standard chemotherapy.[19] Due to the results of *in vitro* cytotoxicity and in *silico* simulation, the inhibition of **1** and **2** on EGFR tyrosine kinase was investigated using **a** commercial radio-labeled kit (Promega, China), with afatinib (Selleck, USA) as the positive control. Compounds **1** and **2** displayed a general inhibition effect on wild-type EGFR tyrosine kinase with IC_{50} values at 28.58 ± 1.37 and 29.13 ± 0.96 μM (Fig. 3C and Table S6†). It gave acceptable consequences coordinated with the cytotoxic and molecular docking results, and suggested that the cytotoxicity of alkaloids **1** and **2** was mediated by the inhibition on EGFR signaling. Natural alkaloids isolated from rot *PN* roots will provide a new scaffold candidate for developing and structural modification of novel EGFR-inhibitor.

Conclusions

Further bioassay-guided phytochemical investigation of rot *PN* roots led to the identification of nine new non-triterpenoids including two alkaloids, and five lactones along with two biotransformed intermediates. Structurally, this study come to a consistent conclusion with our previous work that the oxidation degree was increased in the microbial-infected *PN* roots[5a] from the point of Ginseng polyalkynol. Moreover, compounds **1** and **2** revealed a noteworthy inhibition on five human cancer cell lines. The mechanism of anti-cancer action was explored by target prediction and molecular docking study, which simulated the recognition and interaction of the compounds with amino acid residues of EGFR tyrosine kinase mainly through hydrogen bonds inside the active site of the pocket. Finally, the EGFR inhibition experiment with a moderate inhibition effect verified that the EGFR signaling regulation pathway is probably involved in the anti-cancer cell lines of the active compounds. This work provided a natural candidate for probing and structural modification of novel type EGFR-inhibitor and new anti-cancer agent. Furthermore, the discovery of non-triterpenoid compounds enriched the chemical diversity of *PN* and reminded us that rot *PN* roots can be used as a special resource for bioactive components instead of being wasted or thrown away.

Author contributions

Jia-Huan Shang carried out all the experiments, and prepared the manuscript; Yi-Jun Qiao reviewed and revised the manuscript; Dong Wang and Hong-Tao Zhu participated in the research; Chong-Ren Yang supervised the project; Ying-Jun Zhang designed and directed the project, and revised the manuscript.

Conflicts of interest

There are no conflicts to declare.

Acknowledgements

This work was supported by the Major Science and Technique Programs in Yunnan Province, P. R. China (No. 202203AC100008, 2013FC008, 2016ZF001-01). The authors are grateful to the members of the analytical and bioactivity screening groups at the State Key Laboratory of Phytochemistry and Plant Resources in West China, KIB, CAS, for measuring the spectroscopic data, and cytotoxic and EGFR tyrosine kinase inhibition activities.

Notes and references

1 (*a*) L. P. Christensen, *Adv. Food Nutr. Res.*, 2009, **55**, 1–99; (*b*) L. W. Qi, C. Z. Wang and C. S. Yuan, *Nat. Prod. Rep.*, 2011, **28**, 467–495; (*c*) P. G. Xia, S. C. Zhang, Z. S. Liang and Z. H. Qi, *Chin. Tradit. Herb. Drugs*, 2014, **45**, 2564–2570.

2 (*a*) T. Wang, R. X. Guo, G. H. Zhou, X. D. Zhou, Z. Z. Kou, F. Sui, C. Li, L. Y. Tang and Z. J. Wang, *J. Ethnopharmacol.*, 2016, **188**, 234–258; (*b*) L. F. Huang, H. L. Shi and B. Gao, *Thromb. Res.*, 2014, **133**, 848–854; (*c*) Z. Wang, J. Y. Yang and S. J. Song, *Chin. J. New Drugs*, 2014, **23**, 356–359.

3 (*a*) M. Hisashi, K. Mitsuo, Y. Hiroshi, M. Masato and T. Katsumi, *Chem. Pharm. Bull.*, 1989, **37**, 1279–1281; (*b*) M. Hisashi, *Cancer Chemother. Pharmacol.*, 1995, **4**, 291–296; (*c*) C. M. Teng, S. C. Kuo, F. N. Ko, J. C. Lee, L. G. Lee, S. C. Chen and T. F. Huang, *BBA Gen. Subj.*, 1989, **990**, 315–320; (*d*) M. Kobaisy, Z. Abramowski, L. Lermer, G. Saxena, R. E. Hancock, G. H. Towers, D. Doxsee and R. W. Stokes, *J. Nat. Prod.*, 1997, **60**, 1210–1213.

4 (*a*) Z. S. Mao, Y. J. Long, S. S. Zhu, Z. J. Chen, F. G. Wei, Y. X. Zhu and X. H. He, *J. Chin. Med. Mater.*, 2013, **36**, 2051–2054; (*b*) W. F. Luo, S. F. Yu, C. F. He, Z. Y. Li, C. L. Wang and X. M. Cui, *Acta Phytopathol. Sin.*, 1997, **27**, 85–91.

5 (*a*) J. H. Shang, W. J. Sun, H. T. Zhu, D. Wang, C. R. Yang and Y. J. Zhang, *J. Ginseng Res.*, 2020, **44**, 405–412; (*b*) J. H. Shang, G. W. Xu, H. T. Zhu, D. Wang, C. R. Yang and Y. J. Zhang, *Nat. Prod. Bioprospect.*, 2019, **9**, 287–295.

6 Y. M. Shi, W. I. Xiao, J. X. Pu and H. D. Sun, *Nat. Prod. Rep.*, 2015, **32**, 367–410.

7 M. Kurz, P. Schmieder and H. Kessler, *Angew. Chem.*, 1991, **103**, 1341.

8 R. F. Ma, K. Hu, W. P. Ding, B. Wang, T. B. He, X. N. Li, H. D. Sun and P. T. Puno, *Phytochemistry*, Elsevier, 2021, vol. 182, p. 112589.
9 U. Goergens and M. P. Schneider, *Tetrahedron: Asymmetry*, 1992, **3**, 831.
10 L. L. Lin, Z. L. Chen, X. Yang, X. H. Liu and X. M. Feng, *Org. Lett.*, 2008, **10**, 1311–1314.
11 M. Kobayashi, T. Mahmud, T. Umezome, W. Wang and I. Kitagawa, *Tetrahedron*, 1997, **53**, 15691–15700.
12 (*a*) W. Lu, G. R. Zheng, D. X. Gao and J. C. Cai, *Tetrahedron*, 1999, **55**, 7157–7168; (*b*) M. Satoh, M. Ishii, M. Watanabe, K. Isobe, T. Uchiyama and Y. Fujimoto, *Chem. Pharm. Bull.*, 2002, **50**, 126–128.
13 B. Y. Wang, X. Q. Yang, M. Hu, L. J. Shi, H. Y. Yin, Y. M. Wu, Y. B. Yang, H. Zhou and Z. T. Ding, *J. Ginseng Res.*, 2020, **44**, 770–774.
14 K. Nepali, S. Sharma, M. Sharma, P. M. S. Bedi and K. L. Dhar, *Eur. J. Med. Chem.*, 2014, **77**, 422–487.
15 (*a*) Y. Yatabe and T. Mitsudomi, *Pathol. Int.*, 2007, **57**, 233–244; (*b*) A. Ayati, S. Moghimi, S. Salarinejad, M. Safavi, B. Pouramiri and A. Foroumadi, *Bioorg. Chem.*, 2020, **99**, 103811.
16 (*a*) C. A. Lipinski, F. Lombardo, B. W. Dominy and P. J. Feeney, *Adv. Drug Delivery Rev.*, 1997, **23**, 3–25; (*b*) D. F. Veber, S. R. Johnson, H. Y. Cheng, B. R. Smith, K. W. Ward and K. D. Kopple, *J. Med. Chem.*, 2002, **45**, 2615–2623.
17 D. S. Krause and R. A. Van Etten, *N. Engl. J. Med.*, 2005, **353**, 172–187.
18 (*a*) H. H. Sedlacek, *Drugs*, 2000, **59**, 435–476; (*b*) P. A. Schwartz and B. W. Murray, *Bioorg. Chem.*, 2011, **39**, 192–210.
19 G. A. Masters, S. Temin, C. G. Azzoli, G. Giaccone, S. Baker, J. R. Brahmer, P. M. Ellis, A. Gajra, N. Rackear, J. H. Schiller, T. J. Smith, J. R. Strawn, D. Trent and D. H. Johnson, *J. Clin. Oncol.*, 2015, **33**, 3488–3515.